EFDA–JET–CP(11)04/12

S. Jachmich, T. Eich, G. Arnoux, S. Brezinsek, S. Devaux, W. Fundamenski,
C. Giroud, H.R. Koslowski, Y. Liang, G. Maddison, H. Thomsen
and JET EFDA contributors

# Power Fluxes to Plasma-Facing Components in ELM-Mitigated H-mode Discharges on JET

# Power Fluxes to Plasma-Facing Components in ELM-Mitigated H-mode Discharges on JET

S. Jachmich[1], T. Eich[2], G. Arnoux[3], S. Brezinsek[4], S. Devaux[2], W. Fundamenski[3], C. Giroud[3], H.R. Koslowski[4], Y. Liang[4], G. Maddison[3], H. Thomsen[2] and JET EFDA contributors*

***JET-EFDA, Culham Science Centre, OX14 3DB, Abingdon, UK***

*[1]Laboratory for Plasma Physics, Ecole Royale Militaire/Koninklijke Militaire School, EURATOMAssociation "Belgian State", Brussels, Belgium, Partner in the Trilateral Euregio Cluster (TEC)*
*[2]Max-Planck Institut fuer Plasmaphysik, Euratom Association, Garching, Germany*
*[3]EURATOM-CCFE Fusion Association, Culham Science Centre, OX14 3DB, Abingdon, OXON, UK*
*[4]Institut für Energieforschung - Plasmaphysik, TEC, EURATOM-FZJ, Juelich, Germany*
** See annex of F. Romanelli et al, "Overview of JET Results", (23rd IAEA Fusion Energy Conference, Daejon, Republic of Korea (2010)).*

Preprint of Paper to be submitted for publication in Proceedings of the 38th EPS Conference on Plasma Physics
Strasbourg, France
(27th June 2011 - 1st July 2011)

## 1. CHARACTERISATION OF ELMS

ELMy H-mode is foreseen as one of the scenarios for Q = 10 operating in ITER. The accompanying transient heat loads to the divertor are an urgent issue for both ITER and the metallic wall which is presently under construction at JET. Commonly, ELM-mitigation techniques are aiming at achieving higher ELM frequencies to benefit from the favourable inverse ELM-energy scaling, $dW_{ELM} \propto f_{ELM}^{-1}$. In recent JET-campaigns, Resonant-MagneticPerturbation (RMP) fields [1, 2], impurity seeding [3, 4] and strong gas puffing have been compared as active ELM-mitigation techniques. All ELM-mitigation techniques are associated with some degradation of the pedestal pressure and subsequently reduction of confinement, typically in the order of 10-15%. The large surface temperature rise at the divertor targets during ELMs can cause deterioration of the plasma facing materials. A heat pulse onto a solid body leads to an increase of the surface temperature, which can be characterized by a so-called divertor –heat-flux factor $\eta_{ELM}$:

$$\Delta T_{surf} \propto \eta_{ELM} = E_{ELM} / (A_{wetted} \sqrt{t_{dur}}) \quad (1)$$

with $E_{ELM}$ as energy deposited during the ELM over the wetted area $A_{wetted}$ and during the time $t_{dur}$. As shown in [5, 6] the deposition profile at the outer target, as measured by an IRdiagnostic, broadens during the ELM. Typically from a SOL-width at midplane of about 4.0–6.5mm to about 12–19mm during the ELM. In addition the strike point moves outward, which helps spreading the power over a larger area. Therefore, an effective wetted area during the ELM has been determined using the following definition:

$$A_{wet} = E_{ELM} / \varepsilon_{ELMmax} \quad (2)$$

with $\varepsilon_{ELM,max}$ as the maximum of the energy density profile, calculated as $\varepsilon_{ELM,}(R) = \int_{start}^{end} Q_{surf}(R,t)\, dt$ with $Q_{surf}$ being the heat flux to the tile surface. The end time of the ELM has been defined as two decay times after the peak of the power to the target. The analysis of $\eta_{ELM}$ over a large range of ELM-size, using above definitions, has shown that the maximum surface temperature measured at the target is well represented by this heat flux factor.

## 2. COMPARISON OF ELMS IN GAS-FUELLED PLASMA WITH RMP-MITIGATED ELMS

The results reported here refer to plasma pulses with $I_p = 2.0$MA, $B_t = 1.9$T, $q_{95} = 3.2$, $P_{NBI} = 9.0$MW in a low triangularity shape ($\delta \approx 0.26$). The EFCCs were operated in n = 1-mode. During the Type I ELMy H-mode flat-top phase of the discharge, the EFCC coils have been energised with currents up to 1.5kA*16turns. In addition gas fuelling in the range from unfuelled up to $2.0\times10^{22}$ el/sec have been applied in phases with and without EFCCs. Figure 1 shows the ELMwetted area according to Eq. (2) (triangles) and for the inter-ELM profile (squares) determined for pulses with without fuelling (open symbols), with gas-fuelling (closed symbols), with (red symbols) and without EFCCs (blue

symbols). For the unfuelled, unmitigated ELMs (blue open symbols) one noticed an increase of $A_{wet,ELM}$ with respect to the inter-ELM value by a factor of four. However, for ELMs, which have less energy, the ELM-wetted area decreases as it can be inferred from the gas-scan (blue closed triangle). Applying the EFCCs leads to ELM with much lower ELM-energies (red closed triangles). Most noticeable however is that the inter-ELM deposition area nearly doubles with respect to unmitigated ELMs. In general $A_{wet,ELM}$ ($E_{ELM,out}$) of the mitigated ELMs and unmitigated follows a liner-offset like dependence on ELM size similar as for unmitigated ELMs. The heat-flux factor, which is relevant for the material limits, therefore changes with ELM size. As shown in figure 2, the correlation between $\eta_{ELM}$ and ELM-size, represented by the energy deposited at the target, is remarkably linear. Furthermore, there is no significant different in the scaling of $\eta_{ELM}$ with ELM-size between unmitigated and EFCC-mitigated ELMs.

Due to the density pump-out which is an inherent to the operation of the EFCCs at JET, the pedestal pressure and hence energy confinement is degraded. Besides the reduction of the pedestal pressure, which leads to smaller ELMs, there is no additional beneficial effect of ELM-mitigation using EFCCs compared to gas fuelling. This can be inferred from figure 4, where $\eta_{ELM}$ is plotted against the confinement factor $H_{98}$. For both series of gas scans, with and without EFCCs, the heat-flux factor decreases with confinement as the gas fuelling rate increases.

In order to test whether there is a threshold for ELM-mitigation an experiment, where the EFCC-current has been slowly ramped up, was carried out. The results are summarized in figure 5, in which the results from the steady-state gas-scans have been added. Least-square fits, applied separately to the "slow ramp" data (green symbols) and gas scans (blue and red symbols) has revealed scalings for the reduction of $\eta_{ELM}$ with increasing ELM-frequency $f_{ELM}$: $\eta_{ELM} \propto f_{ELM} - 0.27\pm0.02$ for the IEFCC-slow ramp and $\eta_{ELM} \propto f_{ELM} - 0.41\pm0.14$ for the gas-scan. These scalings are less favourable than an inverse linear scaling.

## 3. REDUCTION OF ELM–IMPACT IN IMPURITY SEEDED PLASMA

Nitrogen ($N_2$) has been seeded in order to lower the steady-state power loads to the target and to achieve low electron temperatures in the divertor. Scans of $N_2$-seeding rates (up to $4.7\times10^{22}$el/sec) have been carried out in high-triangularity plasmas ($\delta \approx 0.42$) with $I_p = 2.5$MA, $B_t = 2.7$T, $q_{95} = 3.5$ over a range of $D_2$-fuelling rates up to $2.8\times10^{22}$el/sec. An analysis of the pedestal pressure profile revealed a tendency for the pedestal energy to degrade with increasing deuterium fuelling or nitrogen seeding. If nitrogen is added the pedestal pressure degrades further. As a result, the heat-flux factor is reduced in a similar fashion for pure $D_2$-fuelled (c.f. black symbols in figure 6) and $N_2$-seeded pulses (red symbols in fig.6). Interestingly, pulses at very high N2-seeding rates ($4.7\times10^{22}$el/sec) showed a pedestal degradation of about 30%, whereas $\eta_{ELM}$ dropped by a factor of 5. This is more visible in figure 7, where $\eta_{ELM}$ is shown as a function of nitrogen-seeding rate. Modest seeding of nitrogen has a similar effect as $D_2$ fuelling, i.e. some reduction of $\eta_{ELM}$. However, with the largest $N_2$ seeding $\eta_{ELM}$ decreases significantly.

## SUMMARY AND CONCLUSIONS

The wetted area has been analysed taking into account the strike-point movement and profile broadening and has been seen to increase with ELM size, which is in agreement with earlier observation at DIII-D [7]. Degradation of the pedestal leads to smaller ELM energy and the ELM impact is thus reduced. Similar degradation of pedestal and confinement has been found for mitigated ELMs using EFCCs, gas fuelling and impurity seeding. Regarding the ELM impact on the divertor, no advantage of using EFCCs over other methods, such as gas fuelling or nitrogen seeding, can be reported.

## REFERENCES:


[1]. Y. Liang et al., Nuclear Fusion **50** (2010), 025013.

[2]. E. de la Luna et al., Proc. 36th EPS-conference (2009).

[3]. G. Maddison et al., Journal of Nuclear Materials (2010), doi:10.1016/j.nucmat.2010.08.059.

[4]. C. Giroud et al., 23rd Fusion Energy Conference, Daejon, Korea, submitted to Nuclear Fusion.

[5]. Th. Eich et al., Journal of Nuclear Materials (2011), doi:10.1016/j.nucmat.2010.11.079.

[6]. S. Jachmich et al., Journal of Nuclear Materials (2011), doi:10.1016/j.nucmat.2010.12.015.

[7]. M. Jakubowski et al., Nuclear Fusion **49** (2009), 095013.


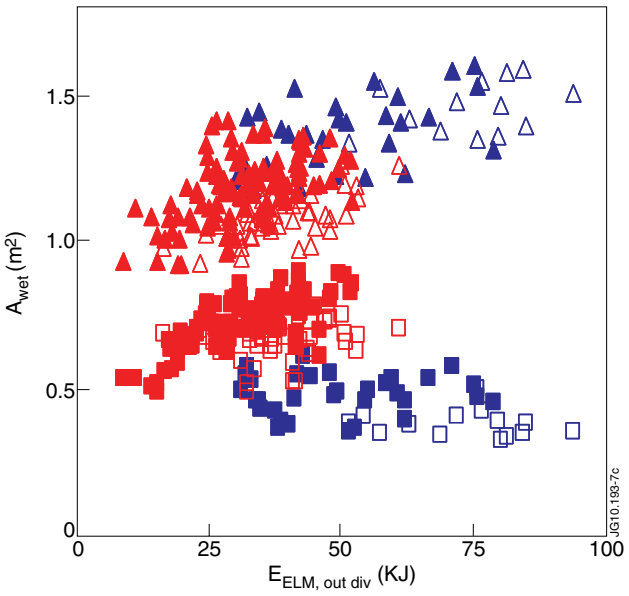


*Figure 1: Wetted area versus ELM energy during ELMs (triangles) and in between ELMs (squares) for unfuelled pulses (open symbols), fuelled (closed) with EFCCs (red) and without EFCCs (blue).*

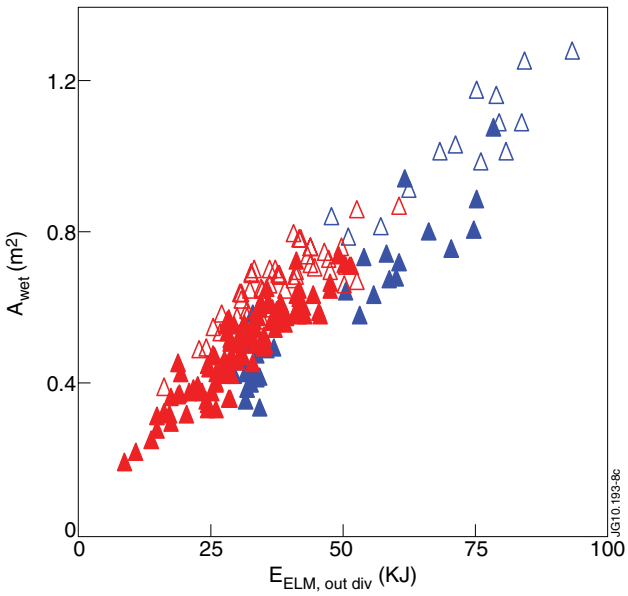


*Figure 2: Heat flux factor as a function of ELM size for the same data set as in figure 1.*

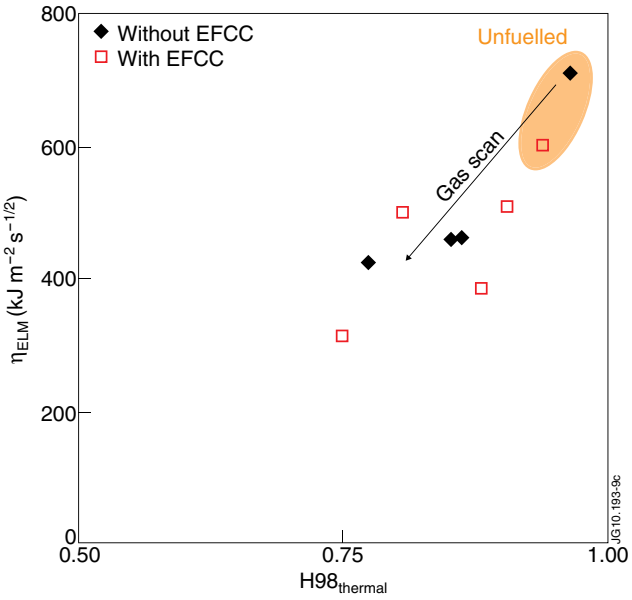


*Figure 3: Heat flux factor versus confinement time normalised to ITER-98(y,2)-scaling.*

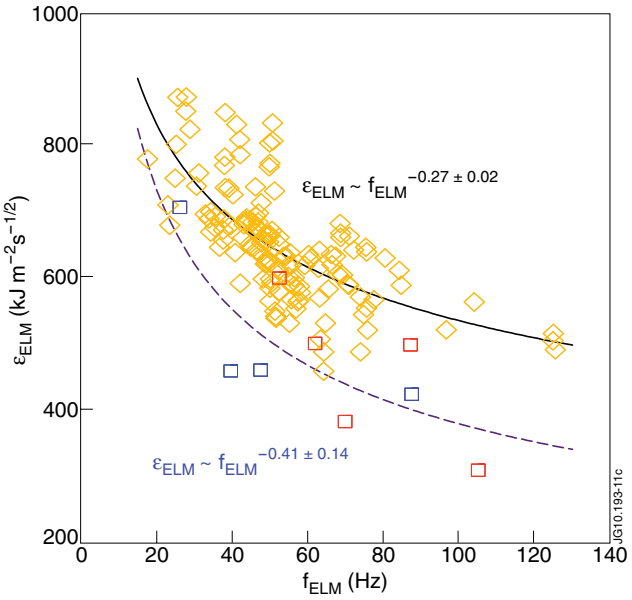


*Figure 4: Reduction of $\eta_{ELM}$ with increasing $f_{ELM}$ for steady state pulses (blue = w/o EFCC, red = with EFCC) and during slow ramp-up of perturbation field (green).*

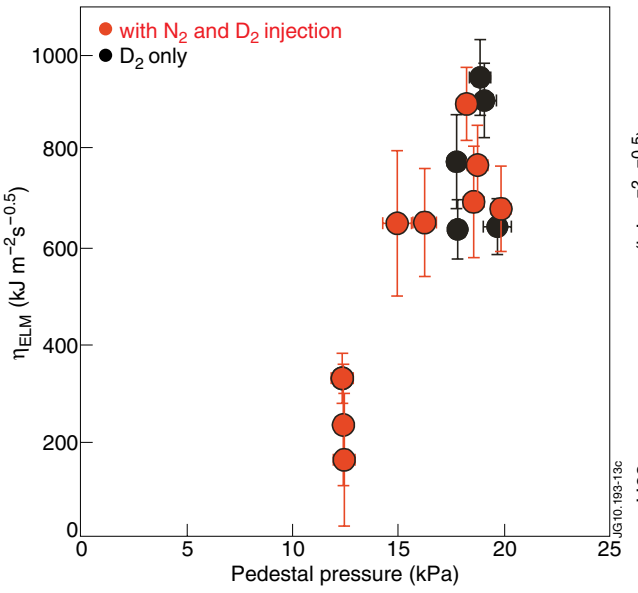


*Figure 5: Effect of pedestal pressure on heatflux factor. The three lowest red points correspond to the highest $N_2$-seeding rate.*

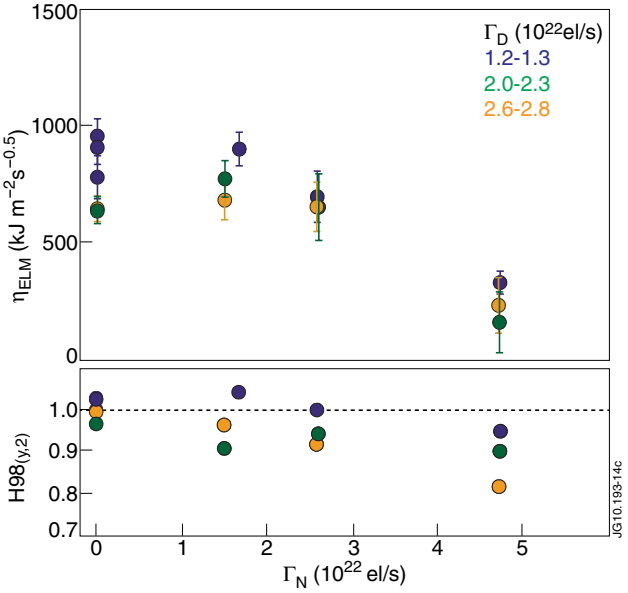


*Figure 6: Heat flux factor (a) and resultung H98(y,2)-factor (b) versus resulting nitrogen seeding rate $\Gamma_N$. The various colors indicate different levels of $D_2$-fuelling.*